Journal of Applied Polymer Science

Electrospun Magnetic Carbon Composite Fibers: Synthesis and Electromagnetic Wave Absorption Characteristics

Ying Yang,[1,2] Zhen Guo,[3] Huan Zhang,[1] Daqing Huang,[3] Jialin Gu,[3] Zhenghong Huang,[3] Feiyu Kang,[3] T. Alan Hatton,[1] Gregory C. Rutledge[1]

[1]Department of Chemical Engineering, Massachusetts Institute of Technology, Cambridge, Massachusetts 02139
[2]Department of Electrical Engineering, Tsinghua University, Beijing 100084, China
[3]Department of Materials Science and Engineering, Tsinghua University, Beijing 100084, China
Correspondence to: Y. Yang (E-mail: yingyang@tsinghua.edu.cn)

ABSTRACT: Electrospun polyacrylonitrile (PAN)-based carbon composite fibers embedded with magnetic nanoparticles have been developed as materials for electromagnetic wave absorption. The nanocomposite fibers were prepared by electrospinning from a dispersion of magnetite (Fe_3O_4) nanoparticles stabilized by L-glutamic acid in a solution of PAN and *N, N*-dimethyl formamide. The Fe_3O_4-embedded PAN nanofibers were stabilized at 270°C in air and carbonized at 800°C in nitrogen. The Fe_3O_4 nanoparticles were crystalline with a particle size of about 7 nm, most of which was reduced to Fe_3C with agglomerates of up to 50 nm diameter in the carbon fibers. The carbon morphology was mostly disordered, but exhibited a layered graphitic structure in the vicinity of the nanoparticles. The carbon composite fiber exhibited ferromagnetic behavior, and the induced magnetic saturation per unit mass of fibers increased with increasing Fe_3O_4 content in the precursor. The complex relative dielectric permittivity was tuned by adjusting the amount of Fe_3O_4 in the carbon fiber precursor. With increasing Fe_3O_4 content, good electromagnetic wave absorption characteristics were observed below 6 GHz, even for samples with fiber loadings as low as 5 wt %. © 2012 Wiley Periodicals, Inc. J. Appl. Polym. Sci. 000: 000–000, 2012

KEYWORDS: fibers; synthesis and processing; nanoparticles; nanowires; nanocrystals; porous materials

Received 25 April 2012; accepted 8 May 2012; published online
DOI: 10.1002/app.38027

INTRODUCTION

Electromagnetic (EM) wave absorption materials have attracted much attention recently for expanded EM interference problems. In general, the performance of EM absorption materials depends on both their dielectric loss and magnetic loss properties.[1] Promising structural carbon-based EM absorption materials that are both load bearing and can absorb EM radiation are receiving increasing attention owing to their superior chemical inertness and thermal stability relative to other materials.[2] Magnetic losses in existing dielectric absorbers can be mediated by incorporating magnetic nanoparticles.[3] The current challenges are to develop lightweight materials with wide absorption frequency, high thermal stability, and resistance to oxidation, for the next generation of EM absorbers.[2]

The classical EM wave absorption materials include powder-like materials and fibrous ones. Carbon black powder and ferrites have been widely studied as they have satisfactory microwave absorption properties, especially for high frequency EM waves above 8 GHz.[1] However, the loading mass in an EM composite absorber can be as much as 10 wt % for carbon black and 80 wt % for ferrites,[1–7] and thus these classical absorbers are of limited use in applications where light weight is essential. Most of the research in this area has been focused on the EM wave absorbing performance of carbon nanotubes (CNT) and metal oxide/CNT composites above 8 GHz.[1–7] However, the preparation of EM absorbers that perform over a wider range of absorption frequencies, especially those below 6 GHz that are important for stealth aircraft technology for long distance (500–600 km) detection, is still a major research challenge.

Carbon fiber (T300 or T700 from Toray) and stainless steel microfibers that are tens of micrometers in diameter are commonly used as fiber absorption materials. However fibers with such large diameters are too large and rigid to be used effectively as components in an EM absorption coating. Where alternating currents are involved, most of the current is carried within a zone near the surface of the fibers, called the "skin depth," which is material-dependent and whose thickness decreases with increasing frequency. For carbon fiber, the skin depth is from 12.6 to 4.1 μm under 2 to 18 GHz,[2] so that

Additional Supporting Information may be found in the online version of this article.

hollow fibers or fibers with diameters less than 4.1 μm could be used as light weight EM wave absorbers without degradation of performance. In recent years, electrospinning technology has emerged as a simple and effective approach to produce nano- to submicron-diameter fibers from either polymer solutions or melts. Subsequent processing to form carbon nanofibers derived from electrospun precursors has also been demonstrated.[8]

Incorporation of metal oxides into electrospun fibers can further enhance their potential applications. Metal oxide/carbon nanocomposite fibers can be prepared either by electrospinning a polyacrylonitrile (PAN)/*N, N*-dimethyl formamide (DMF) solution containing a dissolved metal oxide precursor (such as acetylacetonate salt, $Fe(acac)_3$) for magnetite (Fe_3O_4) followed by carbonization,[8,9] or by the dispersion of previously synthesized metal oxide nanoparticles in PAN/DMF solution just prior to electrospinning and carbonization.[10,11] Most of the electrospun magnetic fibrous mats reported in the literature have been produced based on the first method using DMF as the solvent, because the preparation of a colloidally-stable suspension of magnetite nanoparticles in a strong polar solvent is still problematic. Some Fe_3O_4/polymer nanocomposite fibers have been developed based on the second method, however, especially with polymers that are soluble in aqueous or weakly polar organic solvents (such as chloroform, CH_3Cl). Wang et al., for instance, produced electrospun fibers using colloidally-stable suspensions of magnetite nanoparticles in polyethylene oxide (PEO) and polyvinyl alcohol (PVA) solutions.[12] More recently, Zhang et al.[10] prepared magnetic Fe_3O_4/PAN nanocomposite fibers from DMF/CH_3Cl solutions with suspended Fe_3O_4 nanoparticles, and examined the influence of the operating parameters and the rheological behavior of the solution on the fibers produced. Since DMF is perhaps the most widely used solvent in electrospinning, methods for the preparation of well-dispersed magnetic nanoparticle suspensions in DMF would greatly expand and facilitate the production of other magnetic polymer membranes. Using Triton X-100 as a surfactant, Bayat et al. demonstrated that it is possible to fabricate Fe_3O_4/PAN composite fibers from DMF solution.[11]

In this article, we report the synthesis and characterization of an inexpensive fibrous structure composed of nanometer to submicrometer diameter magnetic carbon composite fibers that show potential as materials for high performance EM absorber applications. Scanning electron microscopy (SEM), transmission electron microscopy (TEM), X-ray diffractometry (XRD), and Raman spectroscopy were used to reveal the microstructure and composition of the composite fibers, while the conductivity of the carbon fibers was measured by impedance spectroscopy. EM wave absorption characteristics were determined to evaluate the EM wave absorption performance of the fibers.

EXPERIMENTAL

Magnetite Nanoparticle Synthesis

The magnetite nanoparticles[12,13] were synthesized from an aqueous solution containing 2.35 g iron(III) chloride hexahydrate, 0.86 g iron(II) chloride tetrahydrate, and 1 g L-glutamic acid prepared by dissolving the reagents in 1 *M* hydrochloric acid, and then mixing the solution with 40 mL of deoxygenated water. Deoxygenation was achieved by bubbling with nitrogen under vigorous stirring for 30 min before reaction. The aqueous solution was heated to 80°C, and 10 mL of 28 wt % of ammonium hydroxide was added to precipitate iron oxide in the form of magnetite. The growth of spherical nanoparticles was arrested by the glutamic acid in the solution, which capped the magnetite nanoparticles shortly after they formed and stabilized them against aggregation. The resulting mixture was then aged for 30 min at 80°C. The final magnetic fluid was washed in a centrifuge to remove excess glutamic acid and salts, and the pH was adjusted to 1 briefly to convert the pendant acid groups to their carboxyl form to ensure a more stable dispersion of the particles in DMF.

Electrospinning Solution Preparation

PAN (M_w = 150 kDa) was purchased from Polysciences (Warrington, PA) and DMF was purchased from Sigma–Aldrich Chemical (St. Louis, MO); both were used as received. Polymer solutions were prepared by adding the PAN polymer directly to DMF and stirring vigorously for at least 3–4 h at 80°C. Various ratios of Fe_3O_4/PAN in DMF were prepared, followed by the addition of PAN/DMF solution to get the desired composition, and by vigorous stirring for at least 24 h at room temperature.

Electrospinning

The parallel-plate electrospinning apparatus used in this study was described earlier by Fridrikh and coworkers.[14] A syringe pump (Harvard Apparatus PHD 2000) delivered polymer solution via a Teflon feed line to a capillary nozzle attached to an upper metal plate. Voltages of up to 30 kV, generated by a power supply (gamma high voltage research ES-30P), were applied between the upper plate and a lower ground plate to provide the driving force for electrospinning. An applied voltage of 22.5 kV, solution flow rate of 1 mL/h, and distance between the capillary nozzle and the collector of 35 cm were found to provide a steady electrospinning operation.

Preoxidation and Carbonization

The preoxidation step was carried out in a box furnace (Lindberg, 1100°C Moldatherm® Box Furnace) by heating the hot-pressed PAN membrane from room temperature to 270°C at a heating rate of 5°C/min in air, and then holding the temperature at 270°C for 90 min to complete the stabilization. The stabilized membrane was then carbonized at 800°C for 1 h in a high purity nitrogen environment in a tube furnace (Lindberg/Blue M 1100°C tube furnace) with a heating rate of 3°C/min. During the heat-treatment, two 0.5-mm thick molybdenum (Mo) plates were used to make a Mo–PAN–Mo sandwich fixed by Mo wire in order to keep the mat flat. No additional pressure was applied to the sample during pre-oxidation or carbonization.[15]

Characterization

The morphology of the electrospun fibers was characterized by scanning electron microscopy (SEM, JEOL-6060). Fiber diameters were determined using AnalySIS image processing software (Soft Imaging System, Lakewood, CO).

A dilute magnetite nanoparticle solution was dried on a carbon grid and visualized under a transmission electron microscope (TEM) (JEM200 CX, JEOL, Japan) to estimate the core sizes of the particles. Cross-sectioned electrospun fibers were also loaded

on TEM grids for TEM analysis. For cross sectional viewing, the fibers were fixed in a glycol methacrylate-based embedding system (JB-4 Plus Embedding Kit, Ted Pella) and then sectioned into 120 nm slices with the diamond knife of an ultramicrotome (RMC Scientific, Tucson, AZ).

For XRD studies, a PANalytical X'Pert Pro multipurpose diffractometer was operated at 45 kV and 40 mA with Cu Kα radiation (wavelength 1.540598 Å) at a scanning speed of 3°/min.

A Horiba Jobin Yvon Labram HR800 spectrometer was used to record the Raman spectra with excitation wavelength 633.0 nm at a laser power of 3 mW.

Magnetization measurements were performed in a vibrating sample magnetometer (VSM, Lakeshore 7404) with an applied field of 10 kOe at room temperature.

In order to analyze magnetite concentration, 0.05 g of Fe_3O_4/PAN fibers was added to a 100-mL volumetric flask, followed by the addition of 0.2 mL 37% hydrochloric acid purchased from Fisher Scientific. The flask was heated using a heat gun for 100 s. The solution turned to yellow since all the Fe^{2+} was oxidized to Fe^{3+}. After cooling the solution to room temperature, 0.3 mL Tiron solution (0.083 g/mL Tiron (Waterstone Technology, LLC) in water) and 1.5 mL of 4*M* NaOH were added to the solution sequentially. Then, the volume of solution was made up to 100 mL with water. The concentration of the Fe_3O_4 in the polymer fiber was determined by the absorbance at 480 nm of the solution on a Cary 100 UV/VIS spectrophotometer. For convenience, throughout this article, we identify samples by the mass ratio (0–17 wt %) of Fe_3O_4 relative to the total mass of Fe_3O_4/PAN as-electrospun fiber; this identification holds also for fibers after stabilization and carbonization.

The samples used for EM absorption measurement were prepared by mixing the carbon fibers with paraffin wax at ratios of 1 and 5 wt %. The complex permittivity and permeability of the composites were measured using the transmission/reflection coaxial line method.[16] The measurement setup consisted of an HP 8722ES vector network analyzer. According to transmission-line theory, the reflection loss (R_C) can be calculated using:

$$R_c = 20\log\left|\frac{Z_I - Z_o}{Z_I + Z_o}\right| \quad (1)$$

$$Z_I = Z_o\sqrt{\frac{\mu}{\varepsilon}}\tan h\left(\frac{i\times 2\pi f}{c}\sqrt{\mu\varepsilon}d\right) \quad (2)$$

where Z_I is the input impedance of the composite sample, Z_o is the output impedance of the composite sample, μ and ε are the complex relative permeability and permittivity, respectively, c is the velocity of light, f is the microwave frequency, and d is the thickness of the composite sample.

RESULTS AND DISCUSSION

The magnetic fibers, as-electrospun and after subsequent stabilization and carbonization, were characterized in terms of their structural and physical properties to ascertain their potential for use as EM absorbing materials, especially for low frequency (<6 GHz) EM waves.

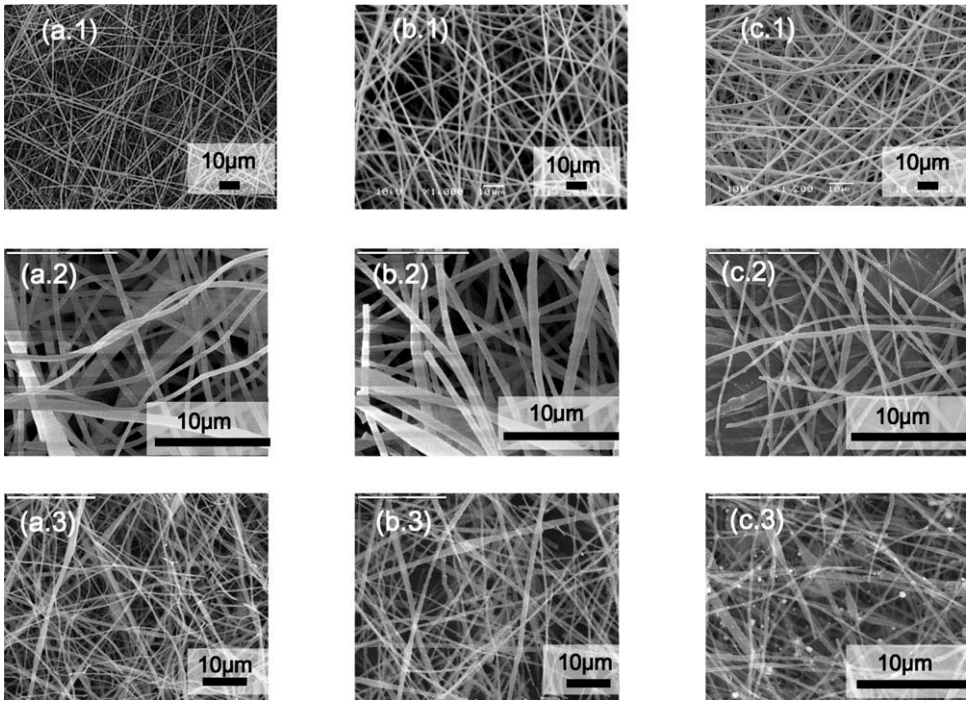

Figure 1. SEM images of electrospun fibers. (a) 2 wt % Fe_3O_4 particle loading in PAN fiber; (b) 7 wt % Fe_3O_4 particle loading in PAN fiber; (c) 17 wt % Fe_3O_4 particle loading in PAN fiber. (1) As-electrospun Fe_3O_4/PAN fibers, (2) fibers after stabilization, and (3) fibers after carbonization.

Applied Polymer SCIENCE

Structural and Compositional Characterizations

SEM Characterization. Magnetic fibers were obtained by the electrospinning of magnetite nanoparticle suspensions in a 10 wt % PAN/DMF solution, with different particle concentrations to ensure final magnetite loadings of 2, 7, and 17 wt % in the resulting solid Fe_3O_4/PAN fibers. For purposes of comparison, neat PAN fibers were also obtained by electrospinning a 10 wt % PAN/DMF solution without any added magnetite. The SEM images in Figure 1 show that the surfaces of the original electrospun fibers were smooth and retained this smoothness after stabilization in air at 270°C. The fibers increased in diameter from 500 to 800 nm to 1.6–2.5 μm with increasing particle loadings in the solution, which can be attributed to the significant increase in the polymer solution viscoelasticity, shown in Supporting Information Figure S1. After carbonization, the fibers shrank to 30 to 40% of their original diameters. Fe_3O_4 particles were observed to reside on the surfaces of the carbonized nanofibers in Figure 3(b.3,c.3). The particle size increases with increasing particle loading in the original as-spun fibers. This phenomenon was also reported in other systems such as tin oxide/carbon fibers during carbonization, which was attributed to growth of the nanoparticles from regions just below the fiber surfaces.[17] The iron oxide nanoparticles themselves grew to form larger particles that broke through the carbon shell and protruded from the fiber surface.

TEM Characterization. The number average nanoparticle hydrodynamic diameter was 146 nm, as determined by dynamic light scattering (DLS). An analysis of the TEM images of as-synthesized magnetite nanoparticles [Figure 2(a)] indicates an average magnetite core diameter of 7.65 ± 1.32 nm. Only the magnetite cores are visible in such TEM measurements because the very low contrast glutamic acid coatings cannot be discerned in these images. The difference between DLS and TEM results is significantly larger than would be anticipated based solely on the presence of the stabilizer coating, indicating that the nanoparticles agglomerated to form clusters in the polymer solutions.

The electron density of the magnetite nanoparticles is significantly higher than that of the PAN matrix, providing a strong contrast and ready visualization of the nanoparticles within the fibers. Figure 2(b, c) show the longitudinal and lateral cross sections of the as-spun fibers with a nanoparticle loading of about 7 wt %. These clusters formed chains within the electrospun fibers, possibly driven by the axial electrical drag force on the PAN along the fiber axis. During carbonization, randomly distributed pores were formed throughout the carbon nanofibers, as shown in Figure 2(d). Some of these pores were empty, and might have been present in the original polymer fiber. Most of the pores, however, contained at least one nanoparticle cluster each, with the size of the particles broadly distributed over the range of 7–50 nm. These particles were smaller than the pores, so that there was residual space around them. Remarkably, Figure 2(e) displays a capsule structure consisting of an iron oxide nanoparticle and graphite layers. The number of graphite layers surrounding any given particle varied, with the thickest coating exceeding 10 layers while the thinnest shell was less than five layers. According to earlier reports,[10,13,18] the graphitization of carbon can be accelerated in the presence of Fe_3O_4; thus the formation of these graphite shells can be explained following the interpretation by Wang et al.[13] used to rationalize the formation of their onion/fullerene-like graphite shells.

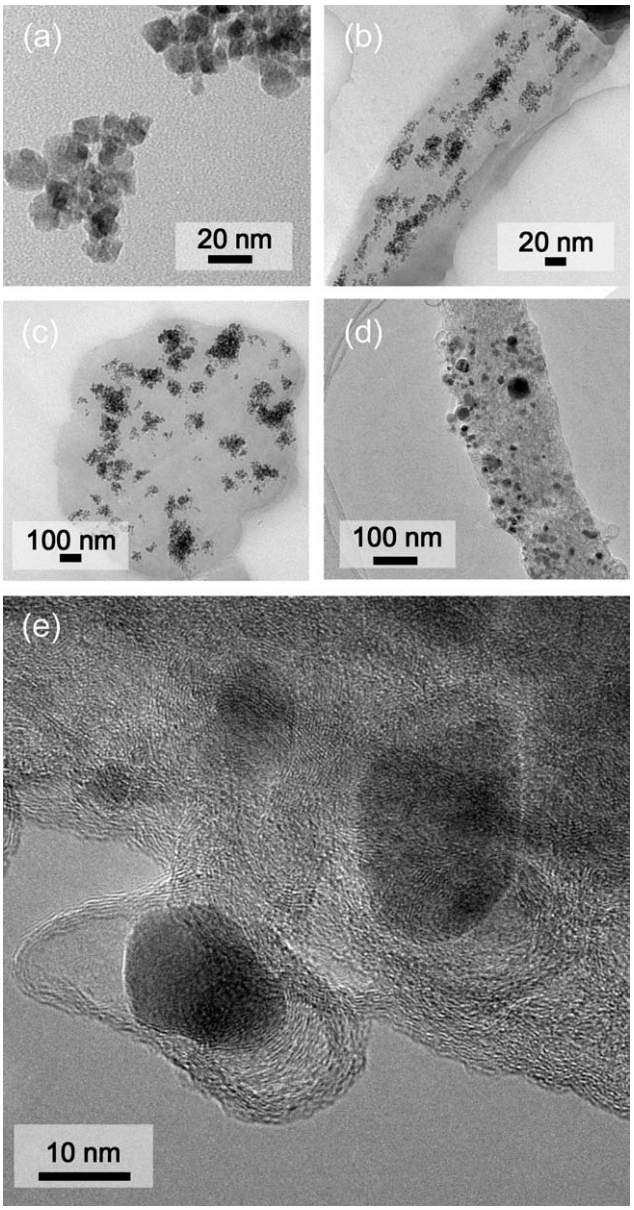

Figure 2. TEM images of (a) the magnetite nanoparticles in DMF; (b) longitudinal cross-section of composite polymer fiber at about 7 wt % Fe_3O_4 loading; (c) lateral cross-section of composite polymer fiber at about 7 wt % Fe_3O_4 loading; (d) carbonized fiber of sample (b) and (c); (e) large magnification image of nanoparticle/carbon fiber with evidence of graphite layer structure.

XRD Characterization. The XRD patterns of Fe_3O_4/PAN composites [Figure 3(a)] show a broad peak at $2\theta = 20°–30°$, which is attributed to noncrystalline material, and a sharp peak at $2\theta = 18°$, which corresponds to the (110) reflection of the orthorhombic PAN unit cell[19]; four additional peaks appear at $2\theta = 35.6$, 43.8, 57.4, and 62.8°, corresponding to the (311), (440), (511), and (400) crystallographic reflections of Fe_3O_4, respectively.[11,15,20]

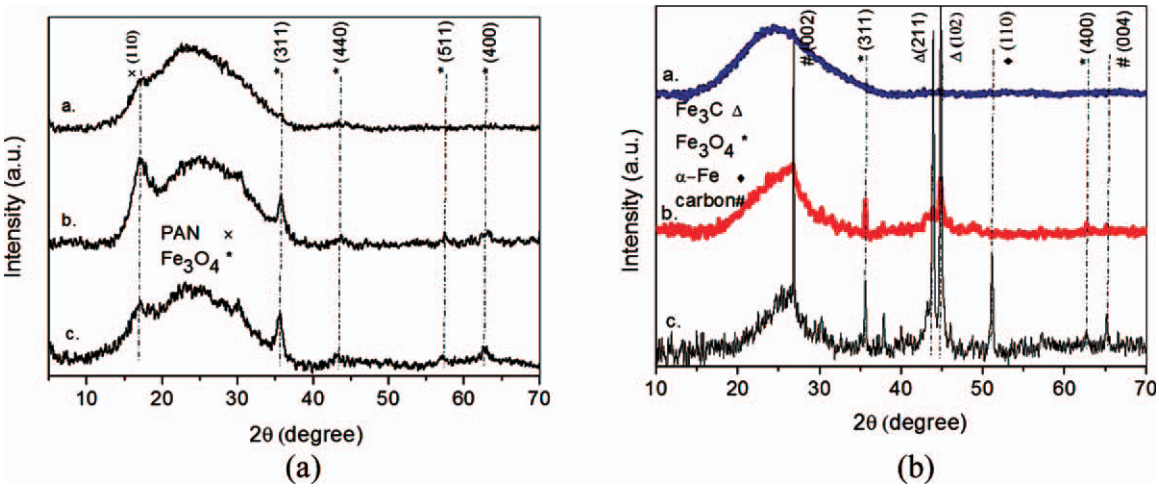

Figure 3. XRD patterns at different Fe_3O_4 loadings: (a) the as-electrospun Fe_3O_4/PAN fiber and (b) the composite carbon fiber. Within each figure, "a" denotes 2 wt % nominal Fe_3O_4 loading, "b" denotes 7 wt %, and "c" denotes 17 wt %. The peaks denoted by "×" are attributed to PAN, the peaks denoted by "*" are attributed to Fe_3O_4, the peaks denoted by "#" are attributed to graphite and the peaks denoted by "Δ" are attributed to Fe_3C. [Color figure can be viewed in the online issue, which is available at wileyonlinelibrary.com.]

PAN-based carbon composite fibers were fabricated by stabilization and carbonization of the electrospun fibers. Figure 3(b) shows the XRD patterns of the composite fibers with different Fe_3O_4 nanoparticle loadings in the precursors, obtained after carbonization at 800°C. The composite fibers showed a very broad diffraction peak around $2\theta = 20°–30°$, which is attributed to the crystallographic (002) plane of graphite in the turbostratic carbon structure.[21] This peak narrowed and shifted slightly towards higher 2θ with increasing (nominal) Fe_3O_4 loadings from 2 to 7 wt %, With a further increase in (nominal) Fe_3O_4 loading from 7 to 17 wt %, two very sharp peaks appeared at 26.7 and 65.1° that are attributed to the (002) plane and (004) plane of graphite, indicating that this higher Fe_3O_4 particle loading can induce a more regular graphite crystal structure around the particles. This is also supported by the TEM image shown in Figure 2(e). Diffraction peaks at 35.6 and 62.8° are observed and assigned to the (311) and (400) crystallographic reflections of Fe_3O_4, respectively.[11,20,22] Fe_3C has also been shown to be formed during the carbonization process, so the observed diffraction peaks at 43.5 and 44.8° likely correspond to the (211) and (102) crystallographic reflections of Fe_3C.[23–25] The additional diffraction peak at 51.1° is due to the α-Fe (110)[25] according to the same sources.[23–25] According to the phase identification by XRD, most of the Fe_3O_4 was converted to Fe_3C.

Raman Characterization. Raman spectroscopy was used to characterize the disordered (turbostratic) versus ordered (graphitic) carbon morphology within the carbonized composite fibers. The peak intensities of the turbostratic structures (I_D, 1350 cm^{-1}) are similar, while those of the ordered graphitic structures (I_G, 1600 cm^{-1}) decrease slightly for carbon fibers with increasing loading of Fe_3O_4 nanoparticles, as shown in Figure 4. The overlap area and graphite peaks are also observed to be narrower for samples with more Fe_3O_4 relative to the pure PAN-based carbon fiber treated under the same conditions. The effective role that Fe_3O_4 plays in enhancing the graphite formation in PAN-based carbon composite fibers is consistent with XRD observations, wherein the (002) graphite peaks are sharper and shifted towards higher 2θ angles.

Electromagnetic Wave Absorption Properties

Magnetic Characterization. The response of the as-spun fiber mat to an applied magnetic field was characterized by measuring its magnetization as a function of the magnetic field strength using VSM. Normalized VSM magnetization curves for composite membranes with 2, 7, and 17 wt % Fe_3O_4 nanoparticles embedded in PAN fibers show superparamagnetic behavior at room temperature [Figure 5(a)], as would be expected

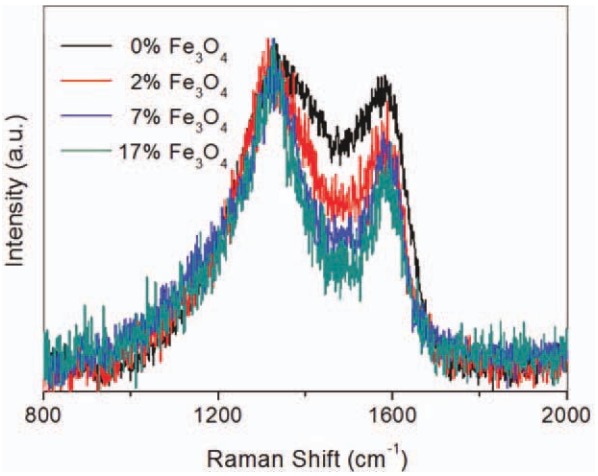

Figure 4. Raman spectra of Fe_3O_4/carbon fibers with different Fe_3O_4 loading. The traces have been rescaled so that the D-band intensity is the same for each sample. From this, it is seen that the G-band intensity decreases (relative to the D band) with increasing Fe_3O_4 content. [Color figure can be viewed in the online issue, which is available at wileyonlinelibrary.com.]

Applied Polymer SCIENCE

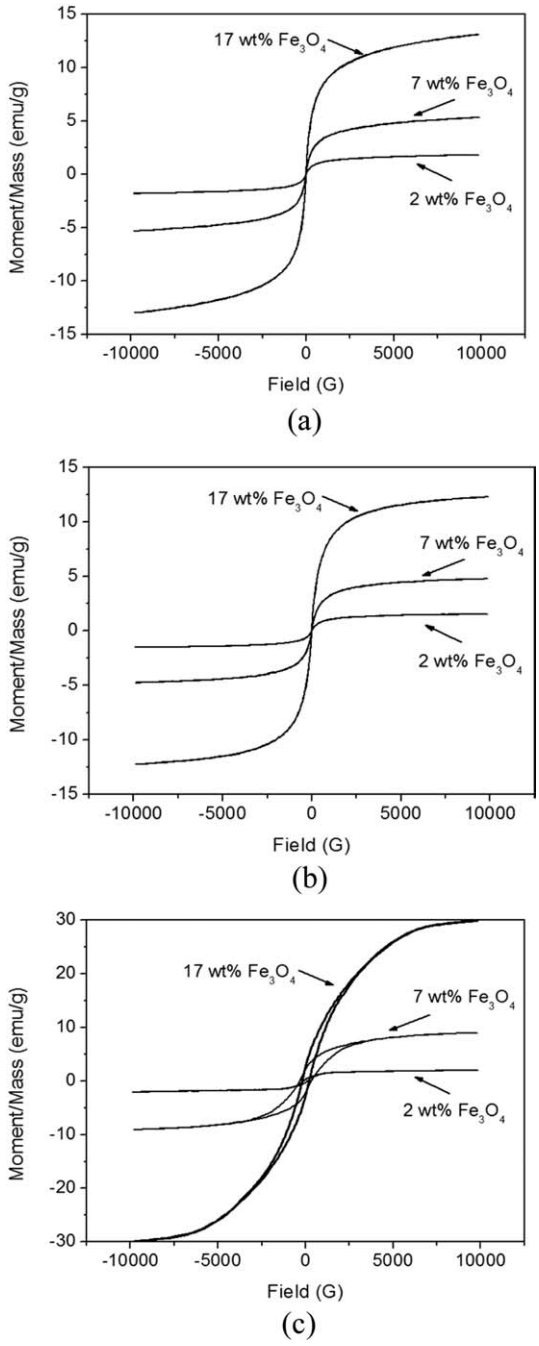

Figure 5. Magnetization versus magnetic field strength for samples with different particle loadings at room temperature. (a) Fe_3O_4/PAN fiber, (b) stabilized Fe_3O_4/PAN fiber, and (c) carbonized magnetic carbon composite fiber.

based on a Neel relaxation time of 10^{-7} s for magnetite particles of mean diameter 7.65 nm.[26] The Fe_3O_4 nanoparticle concentration determines the magnitude of saturation magnetization at higher magnetic field strength. The results show that the induced specific magnetic saturation per unit mass of fiber mat increased from 1.53 to 12.3 emu/g of mat with increasing loading of the nanoparticles from 2 to 17 wt % in the electrospun fibers; this is comparable to the results of Wang et al. for similar loadings of Fe_3O_4 in PEO and PVA.[12] The saturation magnetization for the nanoparticle powder itself was 71 emu/g of particles (c.f. Supporting Information Figure S2). A linear correlation between the saturation magnetization and the wt % loading of nanoparticles was observed. The field dependence of the magnetization of the fibers with different loadings after stabilization is shown in Figure 5(b). It is evident that the electrospun fibers retained their superparamagnetic properties after stabilization, with induced magnetic saturation per unit mass of fiber mat ranging from 1.8 to 13 emu/g of mat as the nominal particle loading increased from 2 to 17 wt % in the fibers. After carbonization, however, the composite fiber exhibited ferromagnetic rather than superparamagnetic behavior, as evidenced by the significant hysteresis in the M-H curves in Figure 5(c). For the carbon composite fiber at nominally 17 wt % particle loading, the saturation magnetization (M_s), retentivity (M_r), and coercivity (H_c) were 30 emu/g, 2.69 emu/g, and 189 Oe, respectively. The enhancement of the saturation magnetization levels in the carbonized samples relative to those in the as-spun and stabilized fibers can be attributed to the carbon fiber weight loss during the carbonization process, as shown in Supporting Information Figure S3, and to the formation of new ferromagnetic phases, such as α-Fe and Fe_3C, as shown in Figure 3. The loss of superparamagnetism may be due to the loss of single domain crystals upon this reorganization and the formation of new phases; both increases in Neel relaxation times associated with larger particles and the formation of multi-domain crystals can lead to hysteresis in the magnetization curves.

Electromagnetic Wave Absorption Characterization. The magnetization curves discussed above demonstrate that the magnetic carbon fibers were ferromagnetic. Here we use the electrospun carbon nanocomposite fiber samples with nominal loadings of 2 and 17 wt % Fe_3O_4 to show the EM absorption potential of these composites. Figure 6 shows the frequency dependence of the real (ε', μ') and imaginary (ε'', μ'') parts of the complex relative dielectric permittivity ε and magnetic permeability μ of the wax composites containing 1 and 5 wt % carbon composite fiber, measured at room temperature. The values of μ' and μ'' remained essentially unchanged with the variations in loading and EM frequency. Since the highest concentration of nanoparticle in the carbon fiber-filled sample for EM absorption test was $\leq$2.4 wt %, corresponding to the sample with 5 wt % of carbon fibers having 17 wt % Fe_3O_4 nominal loading, the contribution of magnetic nanoparticles to the complex relative magnetic permeability was limited. The main contribution of the magnetic nanoparticles in the carbon fibers was to enhance the complex relative dielectric permittivity. The values of ε' and ε'' of the samples increased with higher Fe_3O_4 loadings in the precursor, but decreased with increasing EM frequency. According to the free electron theory,[27] $\varepsilon'' = \sigma/(2\pi f \varepsilon_0)$, where σ is the electrical conductivity. We speculate that the higher ε'' values of the carbon composite fiber at 2–18 GHz are indicative of higher electrical conductivities, attributed to the enhancement of graphitic carbon layers in the fiber due to the presence of the magnetic nanoparticles.

The reflection losses to be expected with composites of sample-thickness 4 mm were calculated using the results of Figure 6(a–c)

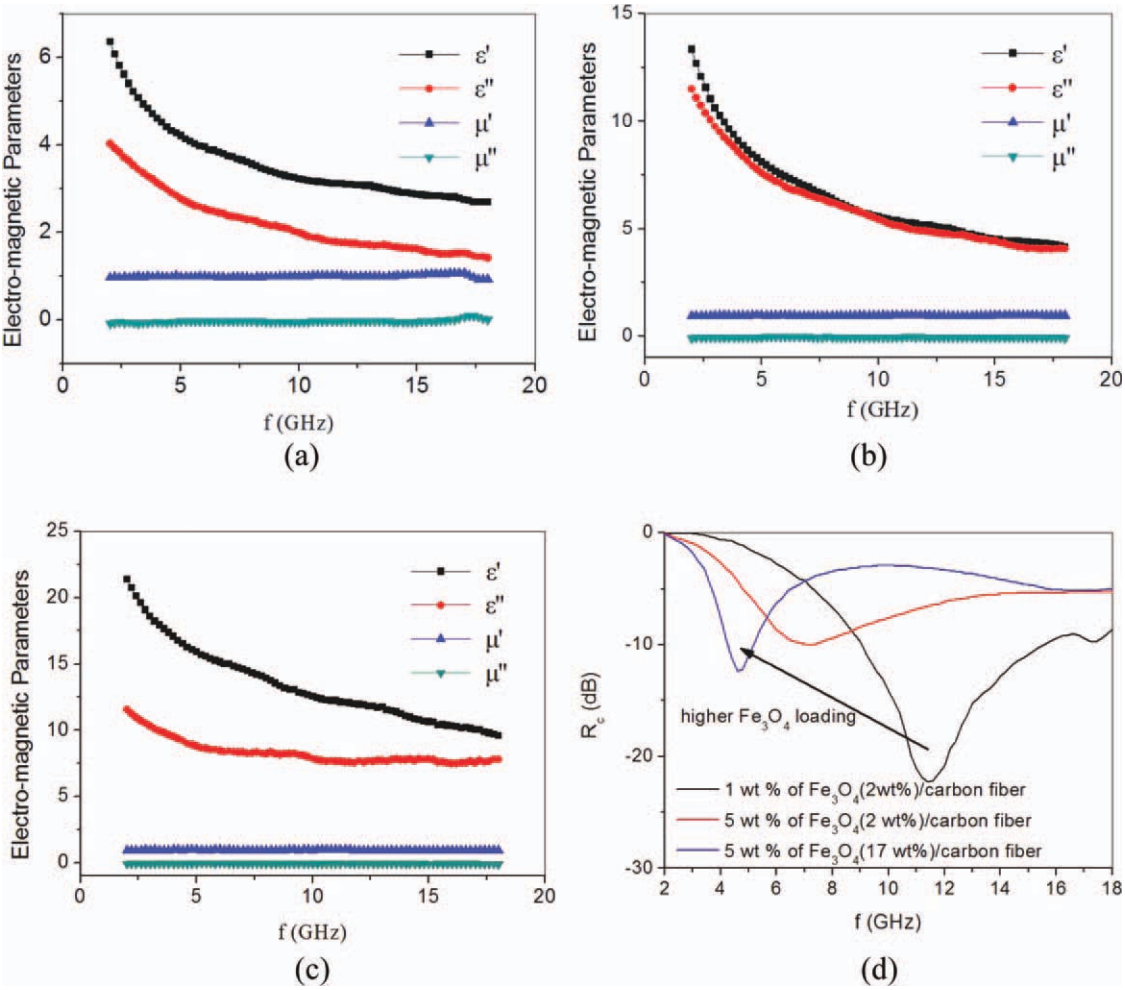

Figure 6. The frequency dependence of the complex relative permittivity and permeability of samples embedded in wax. (a) 1 wt % sample (nominally 2% carbon composite fibers), (b) 5 wt % sample (nominally 2% carbon composite fibers), (c) 5 wt % sample (nominally 17% carbon composite fibers), and (d) calculated reflection loss curves for 4-mm thick EM absorbers based on different Fe_3O_4 loadings in precursor fibers. [Color figure can be viewed in the online issue, which is available at wileyonlinelibrary.com.]

in eqs. (1) and (2) and are shown in Figure 6(d). These calculations indicate that the maximum reflection loss shifts to lower frequencies with higher Fe_3O_4 loadings in the precursors. The frequency region over which the calculated reflection loss falls below −10 dB is 9–16 GHz for a sample with ∼ 0.067 wt % Fe_3O_4 in the carbon fiber-filled sample (1 wt % of carbon fibers with 2 wt % Fe_3O_4 nominal loading in the sample for EM absorption test). For the carbon fiber-filled sample with ∼ 0.33 wt % (5 wt % of carbon fibers with 2 wt % Fe_3O_4 nominal loading in the sample for EM absorption test) and ∼ 2.4 wt % Fe_3O_4 (5 wt % of carbon fibers with 17 wt % Fe_3O_4 nominal loading in the sample for EM absorption test), the frequency regions over which the reflection losses would fall below −5.0 dB are 4.8–18 GHz and 3.5–6.5 GHz, respectively. Thus, even at very low concentrations (<5 wt %), the composite fibers should offer high reflection losses in the low frequency range, a performance that cannot be matched by classical absorbing materials. The low required concentrations of the additive could also be beneficial for the production of lightweight of EM absorbers.

CONCLUSION

PAN-based carbon composite fibers containing magnetic nanoparticles have been synthesized successfully and characterized in terms of properties that are important for their use as EM absorbing materials. The Fe_3O_4 nanoparticles in the fibers enhanced the formation of highly ordered graphitic structures that surrounded the particles. While the electrospun Fe_3O_4/PAN fibers themselves were superparamagnetic, upon carbonization they exhibited magnetic hysteresis, attributed to mass loss and the formation of new iron phases during the heat treatment. Such composite fibers offer good absorption performance in the low frequency ranges, even with less than 3 wt % magnetic nanoparticles in the final composite absorber, which cannot be achieved with traditional absorbing materials. The newly developed low frequency absorption material based on carbon composite fibers could be used in conjunction with other traditional high frequency absorbers, as part of an integrated design. The work reported here points to new opportunities for the targeted

design and tailoring of EM absorption materials with extended absorption ranges and lower mass densities.

ACKNOWLEDGMENTS

This work was supported by the Dupont-MIT Alliance and National Defense Pre-Research Foundation of China (Grant No. 9140A10030110HK5105). We would like to acknowledge Miss. Ting Zhang of Tsinghua University, for helpful discussions on the EM wave absorption characterization.

REFERENCES

1. Petrov, V. M.; Gagulin, V. V. *Inorganic Mater.* **2001,** *37*, 93 (Translated from *Neorganicheskie Materialy* 2001, 37, 135).
2. Micheli, D.; Apollo, C.; Pastore, R.; Marchetti, M. *Compos. Sci. Technol.* **2010,** *70*, 400.
3. Chen, X.; Wei, S.; Gunesoglu, C.; Zhu, J.; Southworth, C. S.; Sun, L. Y.; Karki, A. B.; Young, D. P.; Guo, Z. *Macromol. Chem. Phys.* **2010,** *211*, 1775.
4. Fan, Y.; Yang, H.; Liu, X.; Zhu, H.; Zou, G. *J. Alloy. Comp.* **2008,** *461*, 490.
5. Zou, Y. H.; Liu, H. B.; Yang, L.; Chen, Z. Z. *J. Magn. Magn. Mater.* **2006,** *302*, 343.
6. Zhao, R.; Lei, Y. J.; Meng, F. B.; Zhong, J. C.; Liu, X. B. *J. Magn. Magn. Mater.* **2011,** *323*, 1006.
7. Chen, R. C. *Appl. Phys. Lett.* **2006,** *88*, 66.
8. Wang, L.; Yu, Y.; Chen, P. C.; Zhang, D. W.; Chen, C. H. *J. Power Sources* **2008,** *183*, 717.
9. Panels, J. E.; Lee, J. W.; Park, K. Y.; Kang, S. Y.; Marquez, M.; Wiesner, U.; Joo, Y. L. *Nanotechnology* **2008,** *45*, 455612.
10. Zhang, D.; Karki, A. B.; Rutman, D.; Young, D. P.; Wang, A.; Cocke, D.; Ho, T. H.; Guo, Z. H. *Polymer* **2009,** *50*, 4189.
11. Bayat, M.; Yang, H. J.; Ko, F. *Polymer* **2011,** *52*, 1645.
12. Wang, M.; Singh, H.; Hatton, T. A.; Rutledge, G. C. *Polymer* **2004,** *45*, 5505.
13. Wang, D. W.; Li, F.; Gao, F. L.; Cheng, H. M. *Carbon* **2008,** *46*, 1593.
14. Rutledge, G. C.; Fridrikh, S. V. *Adv. Drug Deliv. Rev.* **2007,** *59*, 1384.
15. Yang, Y.; Simeon, F.; Hatton, T. A.; Rutledge, G. C. *J. Appl. Polym. Sci.* **2012,** *124*, 3861.
16. Park, K. Y.; Han, J. H.; Lee, S. B.; Yi, J. W. *Composites* **2011,** *42*, 573.
17. Zou, L.; Gan, L.; Kang, F. Y.; Wang, M. X.; Shen, W. C.; Huang, Z. H. *J. Power Sources* **2010,** *195*, 1216.
18. Kim, P.; Joo, J. B.; Kim, J. S.; Kim, W. Y.; Song, I. K.; Yi, J. *Korean J. Chem. Eng.* **2006,** *23*, 1063.
19. Hou, X. X.; Yang, X. P.; Zhang, L. Q.; Waclawik, E.; Wu, S. Z. *Mater. Design* **2010,** *31*, 1726.
20. Zou, Z.; Xuan, A. G.; Yan, Z. G.; Wu, Y. X.; Li, N. *Chem. Eng. Sci.* **2010,** *65*, 160.
21. Zhou, Z. P.; Lai, C. L.; Zhang, L. F.; Qian, Y.; Hou, H. Q.; Reneker, D. H.; Fong, H. *Polymer* **2009,** *50*, 2999.
22. Kong, L. R.; Lu, X. F.; Bian, X. J.; Zhang, W. J.; Wang, C. *ACS Appl. Mater. Interfaces* **2011,** *3*, 35.
23. Enayati, M. H.; Seyed-Salehi, M.; Sonboli, A. J. *Mater. Sci.* **2007,** *42*, 573.
24. Kraupner, A.; Antonietti, M.; Palkovits, R.; Schlicht, K.; Giordano, C. J. *Mater. Chem.* **2010,** *20*, 6019.
25. Baltusnikas, A.; Levinskas, R. *Mater. Sci.* **2006,** *12*, 192.
26. Rosensweig, R. E. Ferrohydrodynamics; Cambridge University Press: New York, **1985, p 63.**
27. Zhan, Y. Q.; Meng, F. B.; Lei, Y. J.; Zhao, R.; Zhong, J. C.; Liu, X. B. *Mater. Lett.* **2011,** *65*, 1737.